RSC Advances

This is an *Accepted Manuscript*, which has been through the Royal Society of Chemistry peer review process and has been accepted for publication.

Accepted Manuscripts are published online shortly after acceptance, before technical editing, formatting and proof reading. Using this free service, authors can make their results available to the community, in citable form, before we publish the edited article. This *Accepted Manuscript* will be replaced by the edited, formatted and paginated article as soon as this is available.

You can find more information about *Accepted Manuscripts* in the Information for Authors.

Please note that technical editing may introduce minor changes to the text and/or graphics, which may alter content. The journal's standard Terms & Conditions and the Ethical guidelines still apply. In no event shall the Royal Society of Chemistry be held responsible for any errors or omissions in this *Accepted Manuscript* or any consequences arising from the use of any information it contains.

ROYAL SOCIETY OF CHEMISTRY

www.rsc.org/advances

RSC Advances RSCPublishing

ARTICLE

Structural properties and electrical characteristics of Ho_2O_3 and $HoTi_xO_y$ gate dielectrics for a-InGaZnO thin-film transistors

Cite this: DOI: 10.1039/x0xx00000x

Received 18th April 2014,
Accepted XXth XXX 2014

DOI: 10.1039/x0xx00000x

www.rsc.org/Advances

Tung-Ming Pan,*[a] Ching-Hung Chen,[a] and Jiang-Hung Liu,[a]

In this study, we developed high-κ Ho_2O_3 and $HoTi_xO_y$ gate dielectrics for an amorphous indium-gallium-zinc oxide (a-IGZO) thin-film transistor (TFT) applications. X-ray diffraction atomic force microscopy, and X-ray photoelectron spectroscopy were used to study the structural, morphological and chemical features of Ho_2O_3 and $HoTi_xO_y$ dielectric films. Compared with the Ho_2O_3 dielectric, the a-IGZO TFT incorporating the high-κ $HoTi_xO_y$ gate dielectric exhibited very good electrical characteristics, such as a high $I_{on/off}$ ratio of 1.1×10^8, a high field effect mobility of 20.6 cm^2/V-s, a low threshold voltage of 0.23 V, and a low subthreshold swing of 183 mV/decade. These results are probably due to the incorporation of Ti into the Ho_2O_3 film, resulting in the formation of a smooth surface and a low density of interface states at the oxide/channel interface. In addition, the stability of high-κ Ho_2O_3 and $HoTi_xO_y$ a-IGZO TFTs was investigated under positive gate-bias stress (PGBS) and negative gate-bias stress (NGBS). The electron charge trapping at the dielectric–channel interface resulted from the PGBS, whereas the oxygen vacancies occurred in the a-IGZO under the NGBS.

Introduction

Amorphous oxide semiconductors (AOS) is actively researched for applications to transparent electronics, backplanes of large area active matrix organic light-emitting diode displays, and liquid-crystal displays.[1-3] Among of various AOS materials, amorphous indium-gallium-zinc oxide (a-IGZO) is considered one of the most promising channel materials for thin-film transistors (TFTs) because of its high field-effect mobility (μ_{FE}), low leakage current, good uniformity and stability, high transparency to visible light, and low process temperature.[2-7] In order to obtain excellent device performance, a-IGZO materials with high carrier mobility are critical. Moreover, a high-capacitance gate dielectric is also desired to achieve a low operating voltage to reduce the device power consumption. Insulating silicon dioxide (SiO_2) has been traditionally used as the gate dielectric material in IGZO TFTs. However, SiO_2 with a moderate dielectric constant (3.9) is not an ideal material for high-capacitance gate dielectric. In addition, SiO_2 thin film easily induces higher leakage current due to direct tunnelling through the film,[8] which makes it difficult to obtain high-performance IGZO TFTs. Therefore, search for stable and high-capacitance gate dielectric to replace SiO_2 is currently one of the most important tasks and challenges in IGZO TFTs. High dielectric constant (high-κ) materials as a gate dielectric have been investigated to maintain the high capacitance density and inhibit the gate direct tunnelling current.[9-12] In addition to the electrical requirements, such as a high dielectric constant, low gate current, low interface state density, and good thermal stability, are also very important for high-κ materials. IGZO TFTs featuring high-κ materials such as Al_2O_3, Ta_2O_5, or HfO_2 were already reported in the literature.[13-15] Given the physical deposition processes, interface quality is expected to be considerably worse than the one achieved with the conventional SiO_2.[12] Most of high-κ dielectrics present a polycrystalline structure and have a rough surface, leading to reduced reliability and degraded interface properties.[8,16]

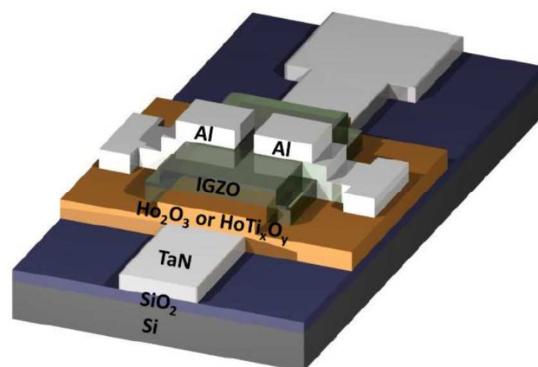

Fig. 1 Three-dimensional view of the high-κ Ho_2O_3 and $HoTi_xO_y$ a-IGZO TFT devices.

RSC Advances Accepted Manuscript

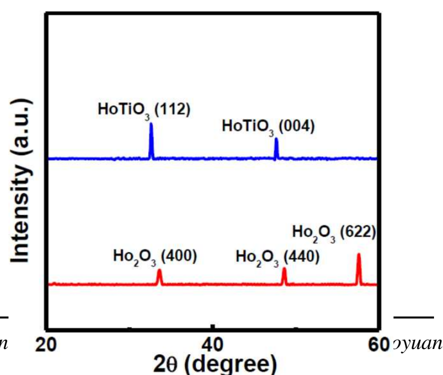

[a]Department of Electron ... yuan 333, Taiwan.
*Corresponding author: Dr. Tung-Ming Pan ;Fax: +886-3-2118507
Tel: +886-3-2118800 Ext. 3349;E-mail: tmpan@mail.cgu.edu.tw

Fig. 2 XRD patterns of Ho_2O_3 and $HoTi_xO_y$ dielectric films.

To solve the problems related with high-κ dielectrics, thin rare-earth (RE) oxides have attracted interest for use as gate dielectrics for TFT applications because they have high dielectric constants and good thermal stability.[17,18] Holmium oxide (Ho_2O_3) film has been studied for gate dielectric applications due to its high κ value, wide bandgap energy, high breakdown field, and low leakage current.[19-22] Exposure to air, however, causes hygroscopic lanthanide oxides to react with moisture to form hydroxides,[23] causing lower values of κ. The incorporation of Ti or TiO_2 films into RE oxides increases their stability toward moisture.[24] Van Dover[25] also demonstrated that the Ti adding RE oxide exhibited excellent electrical performance. Moreover, we reported that $HoTiO_3$ thin film as a gate dielectric showed excellent electrical characteristics such as a high capacitance value, a low density of interface state, a small leakage current, and almost no hysteresis voltage.[26,27] Up to date, the physical and electrical properties of Ho_2O_3 and $HoTi_xO_y$ films as a gate dielectric for a-IGZO TFT devices are still not known. In addition, the reliability and stability are also key concerns for practical TFT applications, and the gate bias stress test is a general method that is used to determine the electrical stability of such an a-IGZO TFT device.[28] In this paper, we compared the structural properties and electrical characteristics of high-κ Ho_2O_3 and $HoTi_xO_y$ gate dielectrics for a-IGZO TFT device applications. We employed X-ray diffraction (XRD), atomic force microscopy (AFM) and X-ray spectroscopy (XPS) to analyze the structural, morphological and compositional changes, respectively, of the Ho_2O_3 and $HoTi_xO_y$ films. Finally, the electrical and reliability characteristics of high-κ Ho_2O_3 and $HoTi_xO_y$ a-IGZO TFTs were investigated.

Experimental

In this study, we fabricated a-IGZO TFT devices with inverted-staggered structures featuring high-κ Ho_2O_3 and $HoTi_xO_y$ gate dielectrics as shown in Fig. 1. The a-IGZO TFT device was fabricated on thermally grown SiO_2 on Si substrate. A 40-nm TaN bottom gate was deposited on the SiO_2/Si substrate by reactive sputtering. A ~50-nm Ho_2O_3 film was deposited on the bottom gate through reactive sputtering from a Ho target in an Ar/O_2 gas ratio of 20/5 at room temperature, while a ~50-nm $HoTi_xO_y$ film was deposited through co-sputtering from both Ho and Ti targets in the same condition. During the sputtering of dielectrics, the dc power of Ho and Ti was 100 and 60 W, respectively, and the chamber pressure was maintained at 10 mtorr. The deposition rate of

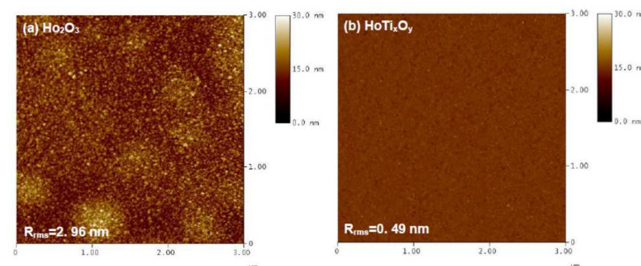

Fig. 3 AFM surface images of Ho_2O_3 and $HoTi_xO_y$ dielectric films. Typical parameters: Scan size=3 μm, Scan rate=1.001 Hz, Data type=height, Number of samples=512, and Data scale=30 nm.

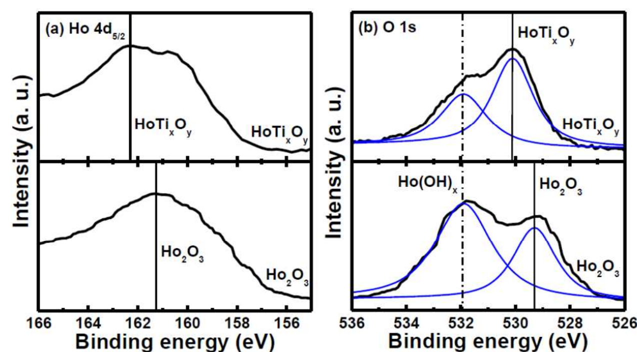

Fig. 4 XPS spectra of (a) Ho $4d_{5/2}$ and (b) O 1s for Ho_2O_3 and $HoTi_xO_y$ dielectric films.

dielectric films was ~0.2 Å/s. Then, samples were subjected to furnace annealing in O_2 ambient for 10 min at 400 °C to form Ho_2O_3 and $HoTi_xO_y$ structures. A 20-nm IGZO active layer was deposited from a-IGZO target (In_2O_3:Ga_2O_3:ZnO= 1:1:1 mol %) by reactive sputtering at room temperature. After the deposition of active channel layer, TFT devices were annealed in N_2 ambient for 10 min 200 °C. Finally, a 50-nm Al film as the source/drain electrodes was deposited by a thermal evaporation system. The active region was defined at the channel width and length (W/L=50 μm/5 μm) by lift-off process.

The crystalline structure and the chemical composition of the Ho_2O_3 and $HoTi_xO_y$ films were investigated using XRD and XPS analyses, respectively. XRD analysis was performed using grazing-incidence Cu K_α (λ = 1.542 Å) radiation. The chemical bonding of the dielectric was determined using a monochromatic Al K_α (1486.7 eV) source. The surface morphology and roughness of the films were analyzed using an NT-MDT Solver P47 (AFM). The AFM was operated in the tapping mode for imaging. The root-mean-square (R_{rms}) roughness was measured from the AFM height images. The dielectric constant and gate leakage of the dielectric films were evaluated from the Al/Ho_2O_3/TaN and Al/$HoTi_xO_y$/TaN capacitors. The capacitance-voltage (C–V) curves of Ho_2O_3 and $HoTi_xO_y$ capacitor devices were measured in the frequency of 1 MHz using a Hewlett-Packard (HP) 4285A LCR meter. The current-voltage (I–V) characteristics of the Ho_2O_3 and $HoTi_xO_y$ a-IGZO TFT devices were measured using a semiconductor parameter HP 4156C.

Results and Discussion

We used XRD to examine the crystalline structures of the Ho_2O_3 and $HoTi_xO_y$ dielectric films, as shown in Fig. 2. The crystalline structure of Ho_2O_3 is body-centered cubic, whereas $HoTiO_3$ film is orthorthombic. A strong $HoTiO_3$ (122) peak and

RSC Advances Accepted Manuscript

 This journal is © The Royal Society of Chemistry 2012

a weak $HoTiO_3$ (004) peak are observed for the $HoTi_xO_y$ sample. In contrast, for the Ho_2O_3 sample, one strong Ho_2O_3 (622) peak and two weak Ho_2O_3 (400) and (440) peaks were found in the 2θ diagram.

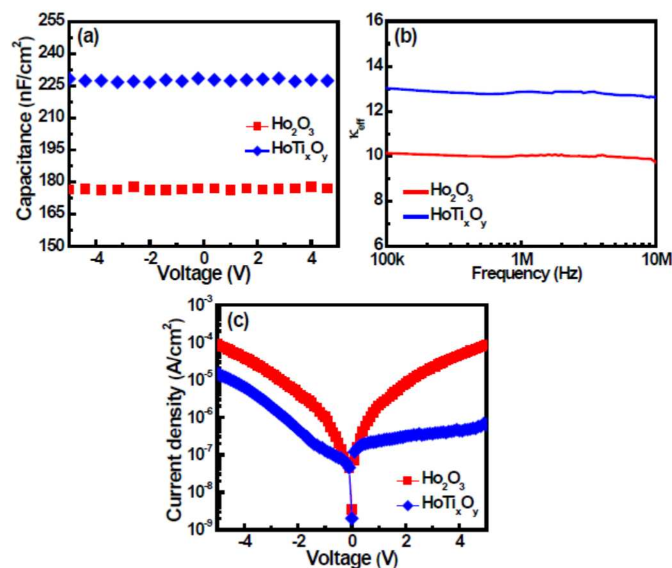

Fig. 5 (a) Capacitance–voltage and (b) κ_{eff}–frequency characteristics of $Al/Ho_2O_3/TaN$ and $Al/HoTi_xO_y/TaN$ capacitor devices. (c) Current–voltage curves of $Al/Ho_2O_3/TaN$ and $Al/HoTi_xO_y/TaN$ capacitors.

Fig. 3(a) and (b) illustrate the AFM images of the Ho_2O_3 and $HoTi_xO_y$ dielectric films, respectively. The surface roughness of Ho_2O_3 film is about three times larger than that of $HoTi_xO_y$ film. It has been reported that oxygen vacancies can exist in the RE oxide films with different charged states,[29] including neutral state, positively charged state, or negatively charged state. The negatively charged oxygen vacancy comprises one electron (V_O^-) or two electrons (V_O^{2-}). These electrons can react with the water by the following reaction equations:

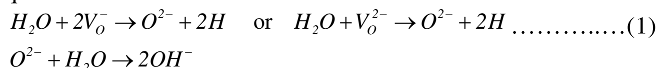

$$H_2O + 2V_O^- \rightarrow O^{2-} + 2H \quad \text{or} \quad H_2O + V_O^{2-} \rightarrow O^{2-} + 2H \quad \ldots\ldots\ldots\ldots(1)$$

$$O^{2-} + H_2O \rightarrow 2OH^-$$

The large surface roughness may be due to the moisture absorption of Ho_2O_3 to form a $Ho(OH)_x$ layer, causing the nonuniform volume expansion of the film.[30] The $HoTi_xO_y$ film has a smooth surface (0.49 nm). The strong resistance to the moisture of $HoTi_xO_y$ film is higher compared with Ho_2O_3 film. This behavior is attributed to the presence of less water reactive TiO_x in $HoTi_xO_y$.[31]

We used XPS to analyze the compositional changes in the Ho_2O_3 and $HoTi_xO_y$ dielectric films. The atomic ratio of Ho:O is 41.1:58.9 in the Ho_2O_3 film, whereas Ho:Ti:O is 24.6:8.7:66.7 in the $HoTi_xO_y$ film. The atomic ratio was determined from the peak intensity areas of XPS spectra. Fig. 4(a) shows the Ho $4d_{5/2}$ XPS spectra of the Ho_2O_3 and $HoTi_xO_y$ films. The Ho $4d_{5/2}$ peaks of the reference Ho_2O_3 located at 161.3 eV.[32] It is found that the Ho 4 $d_{5/2}$ peak of the $HoTi_xO_y$ sample is shifted higher binding energy by about 1 eV as compared to the Ho_2O_3 reference position. We attribute this behavior to the reactions of Ho with the O and Ti atoms to form a $HoTi_xO_y$ structure. Fig. 4(b) displays the O 1s spectra of the Ho_2O_3 and $HoTi_xO_y$ films with appropriate curve-fitting of peaks. Each fitting peak followed the general shape of the Lorentzian–Gaussian function. In the three sets of spectra, the O 1s peaks at 531.9, 530.1, and 529.3 eV represent the Ho–OH,[33] Ho–O–Ti, and Ho–O[34] bonds, respectively. Since hydrogen is more electronegative than Ho metal, the oxygen

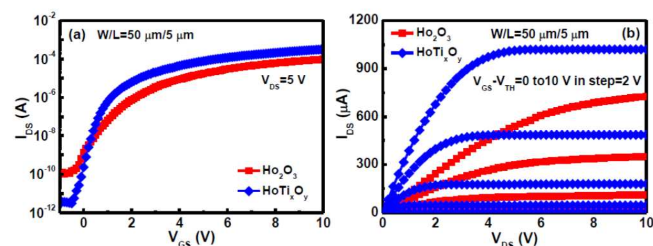

Fig. 6 (a) Transfer (I_{DS}-V_{GS}) and (b) output (I_{DS}-V_{DS}) characteristics of high-κ Ho_2O_3 and $HoTi_xO_y$ a-IGZO TFT devices.

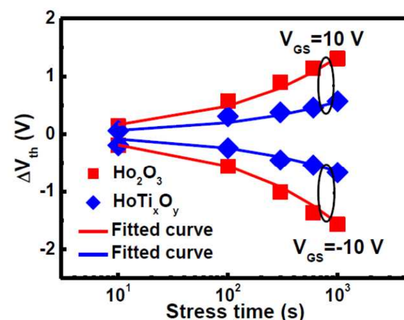

Fig. 7 (a) Threshold voltage shift as a function of stress time for Ho_2O_3 and $HoTi_xO_y$ a-IGZO TFT devices.

atoms in $Ho(OH)_x$ species are less negatively charged than those in the oxide, resulting in a shift toward higher binding energies. The intensity of the O 1s peak corresponding to $Ho(OH)_x$ for $HoTi_xO_y$ sample was lower compared to Ho_2O_3 one. This result can be attributed to the fact that the added TiO_x during cosputtering with Ho_2O_3 increases the oxygen potential to lessen the formation of oxygen vacancies, thus reducing the reaction of water with Ho_2O_3 film. Moreover, the O 1s peak corresponding to $HoTi_xO_y$ had a larger intensity than that of Ho_2O_3. This result may be attributed to the addition of TiO_x into the Ho_2O_3 film reducing in the oxygen vacancies, and thus forming a $HoTi_xO_y$ structure. Therefore, $HoTi_xO_y$ film is a stronger resistance to moisture than Ho_2O_3 one.

Fig. 5(a) shows the C-V curves of the $Al/Ho_2O_3/TaN$ and $Al/HoTi_xO_y/TaN$ capacitor devices. The $Al/HoTi_xO_y/TaN$ device exhibited a higher capacitance density value of 228 nF/cm^2 than $Al/Ho_2O_3/TaN$ one. Fig. 5(b) displays the effective dielectric constant (κ_{eff}) of the Ho_2O_3 and $HoTi_xO_y$ capacitors as a function of frequency. The results show that the κ_{eff} value of Ho_2O_3 and $HoTi_xO_y$ dielectric films keeps around 10 and 13, respectively, at frequency range from 100 kHz to 10 MHz. The $HoTi_xO_y$ film has a higher κ_{eff} value compared with Ho_2O_3 film. This result is due to the large dielectric constant of TiO_x incorporating the Ho_2O_3 film.[16] Fig. 5(c) illustrates the current density–voltage characteristics of the $Al/Ho_2O_3/TaN$ and $Al/HoTi_xO_y/TaN$ devices. It is generally believed that the leakage current of the dielectric film is associated with the surface roughness, crystal defect, and grain boundary.[14] The $Al/Ho_2O_3/TaN$ device exhibited a higher leakage current of 8.8×10^{-5} A/cm^2 at 5 V in comparison with the $Al/HoTi_xO_y/TaN$

RSC Advances Accepted Manuscript

one (6.4×10^{-7} A/cm^2). This result is attributed to the enhancement of leakage conduction path related to the surface roughness, defect states at the interface between channel and insulator layers, and oxygen vacancies in the film. In contrast, a lower leakage current in the $HoTi_xO_y$ film is due to the less defective microstructure and the low surface roughness, as evidenced by AFM image.

Fig. 6(a) shows the transfer characteristics of the high-κ Ho_2O_3 and $HoTi_xO_y$ a-IGZO TFT devices. The threshold voltage (V_{th}) was defined at a fixed normalized drain current ($10^{-9}\times W/L$). The V_{th} of the a-IGZO TFT devices featuring Ho_2O_3 and $HoTi_xO_y$ gate dielectrics is 0.47 and 0.23 V, whereas the $I_{on/off}$ ratio is 9.3×10^5 and 1.1×10^8, respectively. This high $I_{on/off}$ ratio is due to the high capacitance density value and low gate leakage current. In contrast, the low $I_{on/off}$ ratio may be attributed to the rough surface and the presence of oxygen vacancies in the Ho_2O_3 film. Furthermore, the μ_{FE} was determined by the maximum transconductance at constant drain voltage. The μ_{FE} of a-IGZO TFT devices incorporating Ho_2O_3 and $HoTi_xO_y$ gate dielectrics is 15.5 and 20.6 cm^2/V-s, respectively. The high mobility characteristic may be attributed to the smooth surface between the dielectric film and IGZO channel, resulting in the low density of interface states at the dielectric–IGZO interface and small amount of bulk traps in the dielectric. The quality of interface at the dielectric–IGZO of the IGZO TFT can be indirectly evaluated using the subthreshold slope (SS) as is described by the following equation:[35]

$$SS=\left(\frac{2.3kT}{q}\right)\frac{qD_{it}+C_B}{C_{ox}} \quad \text{……………………………………….…(2)}$$

where k is the Boltzmann's constant, T is the absolute temperature, q is the elementary charge, D_{it} is the trap density at the dielectric/channel interface, C_B is the depletion capacitance per unit area, and C_{ox} is the capacitance per unit area of the gate oxide. If we want to turn on the TFT by applying low voltage, we must obtain a small SS value; this demonstrates that a little bias can greatly increase the output current. The small value of SS may be attributed to both the high gate capacitance density and the good interface charge density. The small SS of 183 mV/decade obtained from the IGZO TFTs with a $HoTi_xO_y$ dielectric can be ascribed to the reduced D_{it} at the interface of the IGZO–dielectric because of the smooth surface. On the other hand, the high SS of 520 mV/decade is noticed in the IGZO TFT with a Ho_2O_3 dielectric. The moisture absorption of Ho_2O_3 film may be attributed to the oxygen vacancies in the film and thus increasing its surface roughness. The deposition of IGZO layer on the rough surface produces the high interface trap densities, such as vacancies and dangling bonds, at the IGZO-dielectric interface, which results in SS degradation. The output characteristics of the high-κ Ho_2O_3 and $HoTi_xO_y$ a-IGZO TFT devices are shown in Fig. 6(b). The a-IGZO TFT device using a $HoTi_xO_y$ gate dielectric has a larger driving current compared to Ho_2O_3 dielectric, suggesting the higher mobility and smaller threshold voltage.

Only a few papers have discussed positive gate-bias stress (PGBS) and negative gate-bias stress (NGBS) conditions concurrently,[36] and the relationship of instability of the high-κ Ho_2O_3 and $HoTi_xO_y$ a-IGZO TFTs under PGBS and NGBS conditions is not clear. Fig. 7 depicts the threshold voltage shift (ΔV_{th}) as a function of stress time for the high-κ Ho_2O_3 and $HoTi_xO_y$ a-IGZO TFT devices under PGBS and NGBS. The gate voltage stress was performed at $V_{GS}=\pm10$ V for 1000 s. The positive shift in threshold voltage is due to the fact that accumulated electrons near the dielectric-channel interface were trapped by shallow acceptor-like trap states.[37] Under PGBS condition, the large V_{th} shift (1.31 V) of the a-IGZO TFT device using a Ho_2O_3 dielectric film indicates that more electrons are trapped near/at the dielectric and IGZO interface, while the low V_{th} shift (0.57 V) of TFT device using a $HoTi_xO_y$ dielectric film shows suppressed the trapped charge in the film due to low interface states at the dielectric and channel interface. Moreover, the negative V_{th} shift may be attributed to the fact that the state creation is negligible and more interface states are filled during NGBS. Therefore, the negative V_{th} shift is related to extra free electrons from oxygen vacancies in the IGZO film.[38] The NGBS is more degradation in IGZO TFT than PGBS. To demonstrate the validity of stretched-exponential model to describe the PGBS and NGBS results, we followed a similar methodology that has been developed for PGBS and NGBS experiments.[36] The stretched-exponential model describes the ΔV_{th} by the following formula:[38]

$$\Delta V_{th}=\Delta V_{th0}\left[1-e^{-\left(\frac{t}{\tau}\right)^{\beta}}\right] \quad \text{…………………………………..…..…(3)}$$

where ΔV_{th0} is the threshold voltage shift for infinite time, τ is the constant characteristic trapping time, and β is the stretched-exponential exponent. The ΔV_{th0} value of Ho_2O_3 TFT under PGBS and NGBS is 5.6 and 2.6 V, respectively. The τ value of a-IGZO TFT device under PGBS and NGBS is determined to be 1.1×10^4 and 1×10^4 s, whereas the β value is 0.48 and 0.49, respectively. In contrast, the ΔV_{th0} value of $HoTi_xO_y$ TFT under PGBS and NGBS is 4.9 and 2.2 V, respectively. The τ value of a-IGZO TFT under PGBS and NGBS is evaluated to be 1.2×10^4 and 1.3×10^4 s, while β value is 0.49 and 0.48, respectively. The results were in good agreement with previously reported data.[38]

Conclusions

In this paper, we have successfully demonstrated a high performance a-IGZO TFT device incorporating a high-κ $HoTi_xO_y$ gate dielectric. The a-IGZO TFT device using a $HoTi_xO_y$ gate dielectric exhibited better electrical characteristics, such as a low threshold voltage of 0.23 V, a high $I_{on/off}$ ratio of 1.1×10^8, large field effect mobility of 20.6 cm^2/V-s, and a small SS of 183 mV/decade, in comparison with that of Ho_2O_3 dielectric. We attribute this behaviour to the $HoTi_xO_y$ film forming a smooth surface and reducing the density of interface states at the oxide/channel interface. Moreover, the V_{th} stability on Ho_2O_3 and $HoTi_xO_y$ a-IGZO TFTs was studied under PGBS and NGBS. We found that NGBS is more degradation in a-IGZO TFT than PGBS. The electron charge trapping in the gate dielectric arises from the PGBS, while the oxygen vacancies generated under the NGBS can make a balance of electron trapping for PGBS.

Acknowledgement

This work was supported by the National Science Council, Taiwan, Republic of China, under contract no. NSC-102-2221-E-182-072-MY3.

References

1 H. Yabuta, M. Sano, K. Abe, T. Aiba, T. Den, H. Kumomi, and K. Nomura, H. Hosono, Appl. Phys. Lett., 2006, **89**, 112123.

RSC Advances Accepted Manuscript

This journal is © The Royal Society of Chemistry 2012

2 E. Fortunato, P. Barquinha and R. Martins, Adv. Mater. 24 (2012) 2945.
3 K. Nomura, H. Ohta, A. Takagi, T. Kamiya, M. Hirano, and H. Hosono, Nature, 2004, **432**, 488.
4 J. Jeong, G.J. Lee, J. Kim, and B. Choi, J. Phys. D: Appl. Phys., 2012, **45** , 135103.
5 T. Kamiya, K. Nomura and H. Hosono, Sci. Technol. Adv. Mater., 2010, **11**, 044305.
6 G. H. Kim, B. D. Ahn, H. S. Shin, W. H. Jeong, H. J. Kim, and H. J. Kim, Appl. Phys. Lett., 2009, **94**, 233501.
7 H. Hosono, J. Non-Cryst. Solids, 2006, **352**, 851.
8 G. D. Wilk, R. M. Wallace and J. M. Anthony, J. Appl. Phys., 2001, **89**, 5243.
9 J. S. Lee, S. Chang, S. M. Koo and S. Y. Lee, IEEE Electron Device Lett., 2010, **31**, 225.
10 L. Yuan, X. Zou, G. Fang, J. Wan, H. Zhou, and X. Zhao, IEEE Electron Device Lett., 2011, **32**, 42.
11 N. C. Su, S. J. Wang and A. Chin, IEEE Electron Device Lett., 2009, **30**, 1317.
12 P. Barquinha, L. Pereira, G. Goncalves, R. Martins, E. Fortunato, D. Kuscer, M. Kosec, A. Vila, A. Olziersky, and J. R. Morante, J. Soc. Inf. Display, 2010, **18**, 762.
13 J. I. Song, J. S. Park, H. Kim, Y. W. Heo, J. H. Lee, J. J. Kim, G. M. Kim, and B. D. Choi, Appl. Phys. Lett, 2007, **90**, 022106.
14 C. J. Chiu, S. P. Chang and S. J. Chang, IEEE Electron Device Lett., 2010, **31**, 1245.
15 W. Lim, S. H. Kim, Y. L. Wang, J. W. Lee, D. P. Norton, S. J. Pearton, F. Ren, and I. I. Kravchenko, J. Electrochem. Soc., 2008, **155**, H383.
16 M. Houssa (Eds.), *High-k Gate Dielectrics*, Institute of Physics Publishing, Bristol and Philadelphia, 2004.
17 C. W. Chang, C. K. Deng, J. J. Huang, H. R. Chang, and T. F. Lei, IEEE Electron Device Lett., 2008, **29**, 96.
18 F. H. Chen, J. L. Her, S. Mondal, M. N. Hung, and T. M. Pan, Appl. Phys. Lett., 2013, **102**, 193515.
19 O. Engstrom, B. Raeissi, S. Hall, O. Buiu, M. Lemme, H. D. B. Gottlob, P. K. Hurley, and K. Cherkaoui, Solid State Electron., 2007, **51**, 622.
20 J. Paivasaari, M. Putkonen and L. Niinisto, Thin Solid Films, 2005, **472**, 275.
21 T. M. Pan, W. T. Chang and F. C. Chiu, Thin Solid Films, 2010, **519**, 923.
22 M. Fanciulli and G. Scarel (Eds.), *Rare Earth Oxide Thin Film: Growth, Characterization, and Applications*, Springer, Berlin, 2007.
23 S. Jeon and H. Hwang, J. Appl. Phys., 2003, **93**, 6393.
24 T. Schroeder, G. Lupina, J. Dabrowski, A. Mane, C. Wenger, G. Lippert, and H. J. Mussig, Appl. Phys. Lett., 2005, **87**, 022902.
25 R.B. van Dover, Appl. Phys. Lett., 1999, **74**, 3041.
26 T. M. Pan, L. C. Yen and S. H. Su, Appl. Surf. Sci., 2009, **256**, 1534.
27 T. M. Pan, C. H. Chen, J. H. Liu, J. L. Her, and K. Koyama, IEEE Electron Device Lett., 2014, **35**, 66.
28 R. N. P. Vemuri, W. P. Mathews, M. Marrs, and T. L. Alford, J. Phys. D: Appl. Phys., 2013, **46**, 045101.
29 Y. Zhao, K. Kita, K. Kyuno, and A. Toriumi, Jpn. J. Appl. Phys., 2007, **46**, 4189.
30 Y. Zhao, M. Toyama, K. Kita, K. Kyuno, and A. Toriumi, Appl. Phys. Lett., 2006, **88**, 072904.
31 S. Jeon and H. Hwang, Appl. Phys. Lett., 2002, **81**, 4856.
32 J. F. Moulder, W. F. Stickle, P. E. Sobol, and K. D. Bomben, *Handbook of X-Ray Photoelectron Spectroscopy: A Reference Book of Standard Spectra for Identification and Interpretation of XPS Data*, Physical Electronics. Chanhassen, Mn., 1995.
33 B. S. Jeong, Y. G. Ha, J. Moon, A. Facchetti, and T. J. Marks, Adv. Mater., 2010, **22**, 1346.
34 Y. A. Teterin and A. Y. Teterin, Russ. Chem. Rev., 2002, **71**, 347.
35 S. M. Sze and K. K. Ng, *Physics of Semiconductor Devices* 3rd ed., John Wiley & Sons, 2007.
36 A. Suresh and J. F. Muth, Appl. Phys. Lett., 2008, **92**, 033502.
37 W. T. Chen, S. Y. Lo, S. C. Kao, H. W. Zan, C. C. Tsai, J. H. Lin, C. H. Fang, and C. C. Lee, IEEE Electron Device Lett., 2011, **32**, 1552.
38 J. M. Lee, I. T. Cho, J. H. Lee, and H. I. Kwon, Appl. Phys. Lett., 2008, **93**, 093504.

RSC Advances Accepted Manuscript